



Position Paper

METRIC-GIS: An advanced energy balance model for computing crop evapotranspiration in a GIS environment

J.M. Ramírez-Cuesta^{a,*}, R.G. Allen^b, D.S. Intrigliolo^a, A. Kilic^c, C.W. Robison^b, R. Trezza^b, C. Santos^d, I.J. Lorite^d

^a Dpto. Riego, Centro de Edafología y Biología Aplicada del Segura (CEBAS-CSIC), P.O. Box 164, 30100, Murcia, Spain

^b University of Idaho, Kimberly Research Center, Kimberly, ID, 83341, USA

^c University of Nebraska-Lincoln, Lincoln, NE, 68583-0973, USA

^d IFAPA, Centro "Alameda del Obispo", Alameda del Obispo s/n, Post office box: 3092, 14080, Córdoba, Spain



ARTICLE INFO

Keywords:

Crop coefficient
Evapotranspiration
Modelling
Remote sensing
Satellite
Water requirements

ABSTRACT

A novel ArcGIS toolbox that applies the Mapping Evapotranspiration with Internalized Calibration model was developed and tested in a semi-arid environment. The tool, named METRIC-GIS, facilitates the pre-processing operations and the automatic identification of potential calibration and pixels review. The energy balance components obtained from METRIC-GIS were contrasted with those from the original METRIC version ($R^2 = 1$; $RMSE = 0 \text{ W m}^{-2}$ or mm day^{-1} for ET_c). Additionally, an irrigated scheme located at southern Spain was considered for assessing K_c variability in the maize fields with METRIC-GIS. The identified spatial variability was mainly due to differences in irrigation regimes, crop management practices, and planting and harvesting dates. This information is critical for developing irrigation advisory strategies that contribute to the area sustainability. The developed tool facilitates data input introduction and reduces computational time by up to 50%, providing a more user-friendly alternative to other existing platforms that use METRIC.

1. Introduction

Water is becoming a scarcer resource in many parts of the world due to the increase of human demand and the intensification of competition between water-using sectors (FAO, 2012). In the near future, agriculture will be one of the most affected sectors since it will continue to dominate the withdrawal of water (FAO, 2012). Therefore, a strategic management plan is crucial to preserve and sustain this resource. A prime example is the use of deficit irrigation strategies that have been developed with success in semi-arid environments, reducing the volume of water applied and consumed without affecting the production (Ferreles and Soriano, 2007).

In most cases, proper irrigation management is based on the accurate knowledge of the crop evapotranspiration (ET_c) (Wigmosta et al., 1994; Betts et al., 1997) which expresses the amount of water consumed from a cropped surface in units of water depth (Allen et al., 1998). However, ET_c assessment is not straightforward, and complex procedures and accurate weather data need to be considered to obtain accurate measures or estimation (Allen et al., 1998; Thorp et al., 2019). Numerous

authors have highlighted the advantages of the use of models rather than using field measurements, especially when information over extensive areas is needed (Rana and Katerji, 2000; Drexler et al., 2004; Courault et al., 2005; Senay et al., 2011; Jovanovic and Israel, 2012). In these cases, the FAO56 reference evapotranspiration (ET_0) – crop coefficient approach (Allen et al., 1998) is one of the most widely used models due to its simplicity. However, these types of models provide point estimates that do not account for ET_c spatial variability caused by agronomical practices and that are challenged to estimate accurately reductions in ET_c caused by water shortage. To address this limitation, some authors have integrated the FAO-56 approach with remote sensing technologies in order to create spatially distributed ET maps (Ramírez-Cuesta et al., 2019a).

Crop evapotranspiration maps are generally the basis for irrigation scheduling provided by irrigation advisory services. These irrigation schedules require the consideration of several factors, including the crop water requirements and yield responses to water, the constraints specific to each irrigation method and irrigation equipment, the crop sensitivity to salinity when water of lesser quality is used, the limitations imposed

* Corresponding author.

E-mail address: ramirezcuesta.jm@gmail.com (J.M. Ramírez-Cuesta).

by the water supply and delivery system, and the financial and economic implications of the irrigation practice (Pereira et al., 2007).

Several tools for improving irrigation water management have been developed during the past two decades. Some of these tools have developed user-friendly interfaces for assessing spatially distributed ET maps (Liu, 2009; Raes et al., 2009; Bhattarai and Liu, 2019; Silva et al., 2019) while others have preferred to minimize user interactions to reduce possible human errors by giving options of running multiple simulations (FAO, 2012) or automating the creation of the input and the project files (Lorite et al., 2013). Overall, it is crucial to support the diffusion of technology and improved practices among farmers and technician so that the integration of the tools and internet plays an essential role (Mendicino and Versace, 2007).

Over the last three decades, various remote sensing-based ET_c models have been developed. These models include the Simplified Surface Energy Balance Index (Roerink et al., 2000), Surface Energy Balance System (Su, 2002), Surface Temperature versus Vegetation Index Triangle/Trapezoid Space (Goward et al., 1985; Moran et al., 1994), Surface Energy Balance Algorithm for Land (Bastiaanssen, 1995; Bastiaanssen et al., 1998), Mapping Evapotranspiration with Internalized Calibration (METRIC) (Allen et al., 2007a, b), Two-source N95 model (Norman et al., 1995), and Atmosphere-Land Exchange Inverse model (Anderson et al., 1997). The suitability of these models for ET_c estimation has been demonstrated under different climatic and crop conditions around the world (Nemani and Running, 1989; Kustas et al., 2003; Allen et al., 2005a, 2007b; Bastiaanssen et al., 2005; Poblete-Echeverría and Ortega-Farias, 2012; Santos et al., 2012; Ramírez-Cuesta et al., 2019b). The applicability of these models has been supported by the technological advances in both computer capabilities and algorithm development and automation that have taken place in recent years. There are several software where energy balance models have been incorporated, as the cases of MATLAB (e.g. EvaMapper, Atasever et al., 2013; and LandMOD, Bhattarai and Liu, 2019); R software (e.g. Owusu, 2016) and python environment (e.g. pySEBAL, Hesses et al., 2017). However, despite the undoubted value for users experienced with these type of software, often they are too complex for general application due to the difficulties and tedious algorithms needed to produce estimations (requiring, for instance, programming skills). Therefore, there is an advantage for making these models as accessible and user-friendly as possible by programming them in a common software package to facilitate and optimize ET estimation by any possible user (Lagos et al., 2011).

One of the most widely used ET models is METRIC, which determines ET via a surface energy balance that is based on satellite images containing both short wave and thermal information. METRIC, similar to the SEBAL model, uses hot and cold anchor pixels selected from the satellite image for conditions where a value for sensible heat flux, H, can be reliably estimated (Allen et al., 2007a). Specifically, for METRIC, some tools have been developed to facilitate the selection of the anchor pixels (Kjaersgaard et al., 2009; Allen et al., 2013a). The current, primary METRIC version is implemented in the ERDAS Imagine modelmaker environment (ERDAS Imagine, 2014) that employs an external excel spreadsheet to organize, calculate and assign the parameter values for each specific execution of the model. The modelmaker/spreadsheet combination requires manual control and manual collection of some data, which can result in relatively long processing times, especially when the number of images to be processed is large and/or the areas to be covered are extensive.

Therefore, the main objective of this study was to develop a METRIC remote image-processing model version in the ArcGIS environment that solves some of the main constraints associated with other platforms implementing METRIC model, especially those related to the usability and computational time. This tool provides a faster and a more user-friendly and automated interface for ease in estimating ET for large areas at Landsat satellites spatial resolution. In addition, use of ArcGIS is more common than is the use of the ERDAS system. The new ArcGIS

METRIC tool is demonstrated here for a semi-arid agricultural environment located at Cordoba (Spain), and the results are compared with ET estimates derived using the FAO-56 approach. Several model data management screens are shown to illustrate the model operation.

2. Materials and methods

2.1. METRIC Theoretical Framework

Mapping EvapoTranspiration at high Resolution with Internalized Calibration (METRIC) is a remote sensing-based model that determines ET from satellite imagery by performing a surface energy balance, computing the energy involved in the ET process as a residual of the surface energy equation (Allen et al., 2007a)

$$LE = R_n - G - H \quad (1)$$

where LE is the latent heat flux ($W m^{-2}$); R_n the net radiation flux ($W m^{-2}$); G is the sensible heat flux conducted into the soil ($W m^{-2}$); and H is the sensible heat flux being convected to the air ($W m^{-2}$). The terms on the right-hand side of equation (1) are generally readily estimated using a combination of thermal and short-wave imagery.

The net radiation flux (R_n) represents the radiant energy available for the other energy balance components and is determined based on the balance between the incoming and the outgoing radiant fluxes

$$R_n = R_{S\downarrow} - \alpha R_{S\downarrow} + R_{L\downarrow} - R_{L\uparrow} - (1 - \epsilon_0)R_{L\downarrow} \quad (2)$$

where; $R_{S\downarrow}$ and $R_{L\downarrow}$ are the incoming shortwave and longwave radiation components, respectively ($W m^{-2}$), α is the surface albedo (dimensionless) i.e. the ratio of the reflected to the incident radiant flux over the solar spectrum, $R_{L\uparrow}$ is the emitted outgoing longwave radiation ($W m^{-2}$), and ϵ_0 is the surface thermal emissivity (dimensionless). Procedures for estimating these components are described in Allen et al. (2007a).

The soil heat flux (G) considers the amount of energy conducted into ground and is computed in METRIC by employing the empirical equation developed by Tasumi (2003).

$$G = R_n(0.05 + 0.18e^{-0.521LAI}) \quad LAI \geq 0.5 \quad (3a)$$

$$G = R_n \left(\frac{1.80(T_s - 273.16)}{R_n} + 0.084 \right) \quad LAI < 0.5 \quad (3b)$$

where T_s is the temperature of the surface in Kelvin obtained from a thermal band and LAI is the Leaf Area Index.

Sensible heat flux (H) represents the conductive heat flux from the surface to the atmosphere caused by the difference in air temperature between two near-surface reference heights (Brutsaert, 1982)

$$H = \rho C_p \frac{dT}{r_{ah}} \quad (4)$$

where ρ is the air density ($kg m^{-3}$); C_p is the specific heat of air at a constant pressure ($1004 J kg^{-1} K^{-1}$), r_{ah} is the aerodynamic resistance to heat transport ($s m^{-1}$), and dT is the temperature difference (K) between the two near surface heights (normally 0.1 and 2 m above the zero plane displacement height). dT is calculated as a linear function of T_s as proposed by Bastiaanssen (1995).

$$dT = a + bT_{s \text{ datum}} \quad (5)$$

where a and b are empirical coefficients for a given satellite product determined through the two anchor pixels (i.e. cold and hot pixels) where a value for H can be faithfully estimated, and $T_{s \text{ datum}}$ is the land surface temperature adjusted to a standard elevation datum per pixel of the satellite image (Allen et al., 2007a). The 'delapsing' of T_s is done to remove artifacts in surface temperature that are caused by differences in air pressure, rather than to differences in surface energy balance characteristics.

Once all components of Eq. (1) are determined, ET at the satellite image acquisition time (ET_{inst} , mm h^{-1}) is calculated at pixel level by dividing LE from Eq. (1) by water density ($\rho_w = 1000 \text{ kg m}^{-3}$) and by the latent heat of vaporization (λ , J kg^{-1})

$$ET_{inst} = 3,600 \frac{LE}{\lambda \rho_w} \quad (6)$$

The primary METRIC version was developed in ERDAS (hereafter termed METRIC_{erdas}), requiring manual processing of up to ten sub-models and the use of a data-handling and management spreadsheet to assign the image metafile folder, define the structure of the weather data document (length of weather time period, flag for weather reporting time and to account for daylight savings time, among others), the values for soil-dependent parameters (e.g. soil type, field capacity and wilting point, among others), and other parameters, including the surface roughness of the weather station, the delapsing rate, and various toggles and parameter settings. The ERDAS-version spreadsheet uses Visual Basic Assistant macros to transfer parameter settings from the spreadsheet into the ERDAS modelmaker code (Allen et al., 2005b).

A variety of settings and adjustments can be enabled or disabled in the ERDAS-based spreadsheet. These corrections include (i) an α adjustment to account for the biased lowering of α for deep vegetation when viewed from nadir, as opposed to the full hemispherical α that should be used when computing the surface energy balance; (ii) an adjustment to account for the interception of solar radiation (R_{so}) by microdepressions, and trees (especially for correcting R_{so} on north-facing slopes); (iii) an adjustment to compensate the temperature in those areas where the shadows within the canopy that are viewed from nadir decrease the bulk T_s ; (iv) a reducer to diminish the slope of the dT versus T_s function when T_s is beyond the T_s of a dry, bare tilled field threshold; (v) an adjustment to consider the effects from the orthographic drainage of air caused by cooling, the acceleration of air streams passing over mountains due to the Venturi effect, and the impacts of drag due to undulating topography; (vi) an adjustment to reduce wind levels on leeward slopes; (vii) an adjustment to add an extra resistance to diminish the sensible heat flux as consequence of the influence of sage brush and tall grass vegetation in desert areas that effectively protects the land surface from mechanical heat transport, but is sparse enough to permit the penetration of incoming R_{so} that heats the soil surface; (viii) a toggle to adjust the G function to be adjusted during application to desert soils to account for effects of delamination and differences in porosity, structure and other effects that may reduce the thermal conductivities of the soils and cause the soils to deviate from their agricultural counterparts; and (ix) an adjustment to take into account the energy that may be invested in thawing and warming the soil when soil may have been frozen the previous night. These adjustments and algorithms have been described by Allen et al. (2007a, 2011; 2013b), Irmak et al. (2011) and Kilic et al. (2016).

2.2. METRIC-GIS implementation

In this study, the METRIC_{erdas} and supporting METRIC spreadsheet algorithms were integrated into an ArcGIS toolbox environment using ArcPy language to produce a site-package that performs geographic data analysis, data conversion, data management, and map automation with Python. ArcPy provides access to ArcGIS geoprocessing tools as well as to existing functions, modules, and classes. This allows the development of powerful scripts thanks to its code-completion function and the function-specific reference documentation. Moreover, the use of Python language permits benefiting from the development of additional modules by GIS professionals and programmers.

The METRIC version that was used as a basis was the 2014 version of METRIC that computes ET for flat areas. This version is valid for most agricultural areas due to its generally flat topography and has provided accurate ET estimations similar to those obtained with METRIC versions including Mountain model (Healey, 2011). Hereafter, the METRIC

model integrated into ArcGIS will be denoted as METRIC-GIS in order to distinguish it from METRIC_{erdas}. The tool (together with a sample dataset) will be freely distributed to interested readers by contacting the corresponding author.

The model has been divided into four sub-models, which were created with ArcPy and imbedded into an ArcGIS (v10.2; Esri, Redlands, CA, USA) toolbox, providing a user-friendly and explanative interface to execute the model, where the user only needs to select or provide the values for the required inputs. The first sub-model, “1. Data formulation” (Fig. 1a and b), computes parameters needed to identify candidates for the selection of the ‘anchor’ pixels. The inputs required to run this sub-model are the Landsat folder path description for the Landsat Scene Image downloaded from EROS; a Digital Elevation Model (DEM) image for the Landsat Scene; a raster image describing the land use for the area using the United States Geological Survey (USGS) National Land Cover Database (NLCD) definitions (if another land-use source is used, e.g. CORINE land cover, a previous recoding process is required for matching the NLCD codes); a mask (in shapefile format) that outlines the study area to be processed (optional); a weather data file containing hourly (or shorter) data (see section 2.3.2. *Meteorological Data*); the folder where the resulting rasters and the text file with the summary of the data preparation script will be stored; a folder where an anchor pixel point shapefile will be created if it does not exist; a toggle to enable/disable the α adjustment for tall vegetation and/or tall crops that was explained in the previous section; a toggle used to identify tall vegetation for adjustment of α and partitioning of T_s into canopy and shaded components for forest, trees, and vines; the atmospheric clearness coefficient; a minimum value of α when using a nadir-viewing satellite such as Landsat; the flat and mountain lapse rates and the terrain elevation considered for the lapse rate change; the path radiance for the thermal band; the narrow band downward thermal radiation from a clear sky; the narrow band air transmissivity in the thermal band spectral range; soil water balance-related parameters; a folder containing recommended symbols for output files (optional); and a binary mask for identifying the presence of clouds or shadows (optional). All raster images must have the same raster size and coordinate system as the Landsat images (i.e. Universal Transverse Mercator - World Geodetic System 1984 coordinate system).

Many of these parameters have standard, default values automatically entered into the input menu to expedite data entry. The output raster resulting from this sub-model are ϵ_0 , transmittance, R_{so} , α , Normalized Difference Vegetation Index (NDVI), Normalized Difference Water Index (NDWI), Normalized Difference Snow Index (NDSI), LAI, T_s and a G multiplier to account for organic matter (GxOM). Each parameter entry box has an associated description of the parameter that appears on the help screen to explain the parameter and to recommend common values or ranges of values.

The second sub-model, comprising “2a. Sample Pixel Identification” and “2b. Identified Pixels Sampling” (Fig. 2a and b and 3), is intended for identifying potential pixels/points for calibration sampling from uniform areas and for sampling the DEM, NLCD, transmissivity, R_{so} , α , NDVI, LAI, T_s , and GxOM rasters from the identified/modified sample pixel point shapefile. The inputs required in this sub-model are a summary/log file (text) generated when the data preparation model was run; the anchor pixels shapefile created by the flat model preparation script or generated by the user; a point shapefile with existing pixel sampling points (optional); the distance from the weather station location used in showing “identified pixels” close to the weather station in the map and graph; the neighborhood in which to evaluate the uniformity of the neighborhood surrounding a pixel; The NLCD classes to consider as potential pixels/points for calibration sampling; uniformity ranges for elevation, NDVI, T_s , α and GxOM; minimum and maximum thresholds for α and GxOM; and a folder containing recommended symbols for output files (optional).

Third sub-model, “3. Final Computations” (Fig. 4a and b), calculates the different energy balance components using selected hot and cold

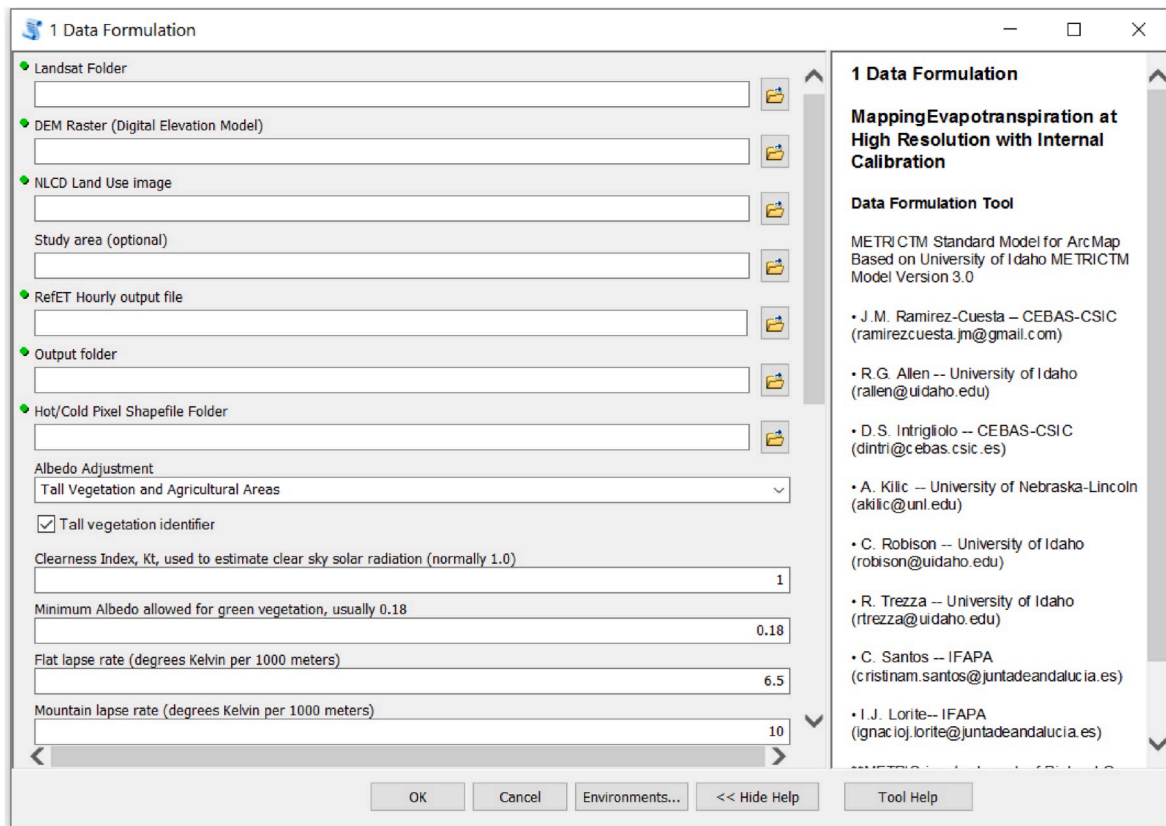


Fig. 1a. Section one of toolbox interface of sub-model 1, “1. Data formulation”, implemented in ArcGIS, showing the different input parameters and standard default parameter values. Readers are referred to the main text for definitions of the abbreviations used in the figure.

pixel locations. Sub-model 3 reads most of its inputs from a text file automatically generated when the first and second sub-models are run. This text file contains the pathnames and other parameters. Sub-model 3 requests entry of information describing a point shapefile indicating the hot and the cold pixel locations; the folder where the resulting raster will be stored; a clump factor; a shape factor and the ratio between the height of the tree and its width used in the three-source partitioning of surface temperature for trees (Allen and Kjaersgaard, 2010); the fraction of tree height from the ground to the lower edge of the tree foliage; the Perrier canopy shape factor for sparse vegetation (Perrier, 1982; Santos et al., 2012); a scaling factor for compensating the temperature in those areas where the shadows within the canopy that are viewed from nadir decrease the bulk surface temperature; a divisor to reduce the slope of the dT versus T_s function when T_s is beyond the T_s of a dry, bare tilled field threshold; a multiplier for adding an extra resistance to diminish the sensible heat flux as consequence of the influence of sage brush and tall grass vegetation in desert areas; a multiplier to adjust momentum roughness length for tall crops or low α ; toggles to enable or disable the adjustments described in section “2.1. METRIC Theoretical Framework”; the temperature used to identify a surface that may have frozen the previous night; a multiplier for adjusting G when soil has been frozen the previous night; the fitting coefficients used to estimate sunlit and shaded T_s in the three-source model for trees; the values of ET_{rF} for the hot and cold pixel; the surface roughness of the weather station; the folder containing recommended symbology for output files map layers; and the point shapefile with points (pixels) to sample the various sub-model 1 output rasters at. The output rasters resulting from this sub-model are R_n , G , H , K_c (referred to ET_0) and ET_c .

Finally, the fourth sub-model, “4. EF Adjustment” (Fig. 5), performs an Evaporative Fraction (EF) adjustment using as inputs a summary/log file (text) generated when the final computations model was run; the folder where the resulting rasters and the text file with the summary of the

adjustment script will be saved; the cold and hot surface Slob coefficients for daytime and for 24 h periods (Allen et al., 2005b); a coefficient for weighting effective day length; the weight to give to the 24 h EF component; and the folder containing recommended symbology for output files map layers.

2.3. Toolbox performance

In order to ensure that METRIC-GIS was successfully programmed and no transcription errors existed, the energy balance components (R_n , G , H and ET) derived from the toolbox were compared with those obtained with METRIC_{erdas}. This comparison was performed on a pixel-by-pixel basis, selecting 100,000 randomly distributed pixels within a Landsat 8 scene (path 201 row 34) corresponding to the DOY 188 (July 7th, 2015). This date was selected due to its high ET_0 (7.87 mm day^{-1}) which allowed evaluation over a wide range of values for all energy balance components, especially for ET_c , whose range can vary from 0 mm day^{-1} , on dry bare soil surfaces, to close to 10 mm day^{-1} in maize fields.

2.4. Practical application

2.4.1. Study area

In order to show the potentiality of the developed tool, METRIC-GIS was tested in a semi-arid environment. The selected area is part of the Genil-Cabra Irrigation Scheme located in Cordoba, Andalusia, in southern Spain ($37^\circ 32.93' \text{ N}$, $4^\circ 49.30' \text{ W}$; Fig. 6). The climate is Mediterranean continental and for the September 2014–September 2015 annual period, the average air temperature and relative humidity were 18.2° C and 64.7%, respectively. Average wind speed was 1.7 m s^{-1} , R_{so} was $17.6 \text{ MJ m}^{-2} \text{ d}^{-1}$, and cumulative ET_0 and precipitation were 1443 and 411 mm, respectively. The predominant soils in the

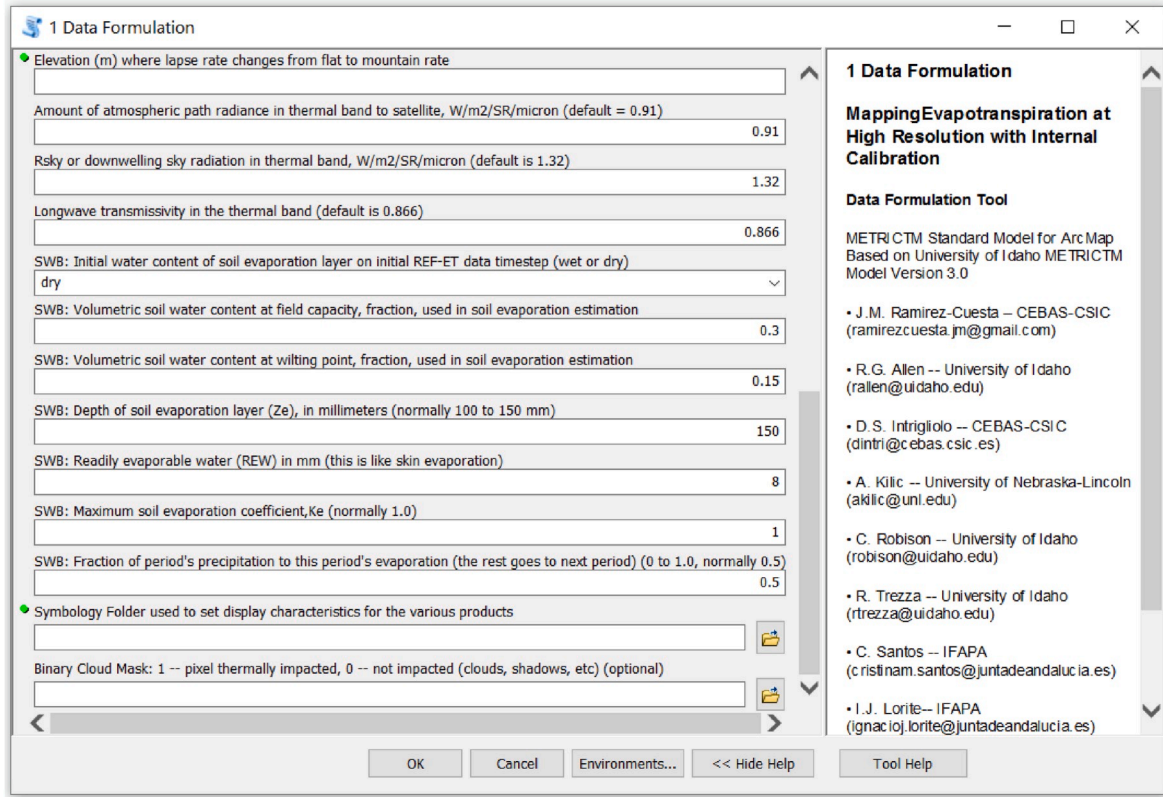


Fig. 1b. Section two of toolbox interface of sub-model 1, “1. Data formulation”, implemented in ArcGIS, showing the different input parameters and standard default parameter values. Readers are referred to the main text for definitions of the abbreviations used in the figure.

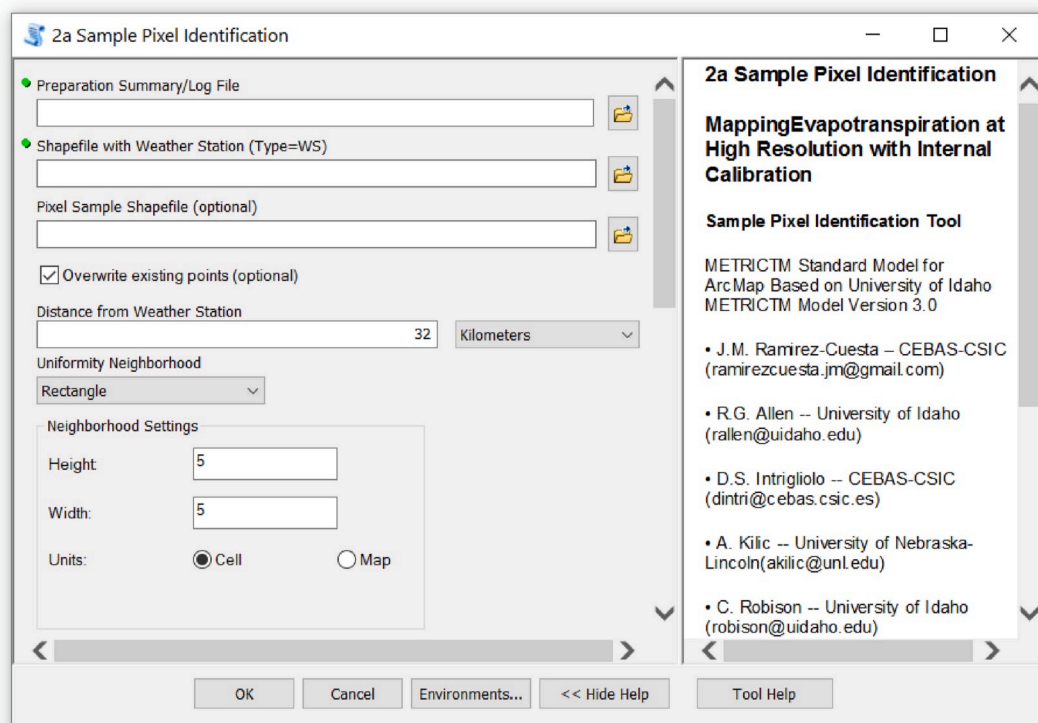


Fig. 2a. Section one of toolbox interface of sub-model 2, “2a. Sample Pixel Identification”, implemented in ArcGIS, showing the different input parameters. For definitions of the abbreviations used in the figure, readers are referred to the main text.

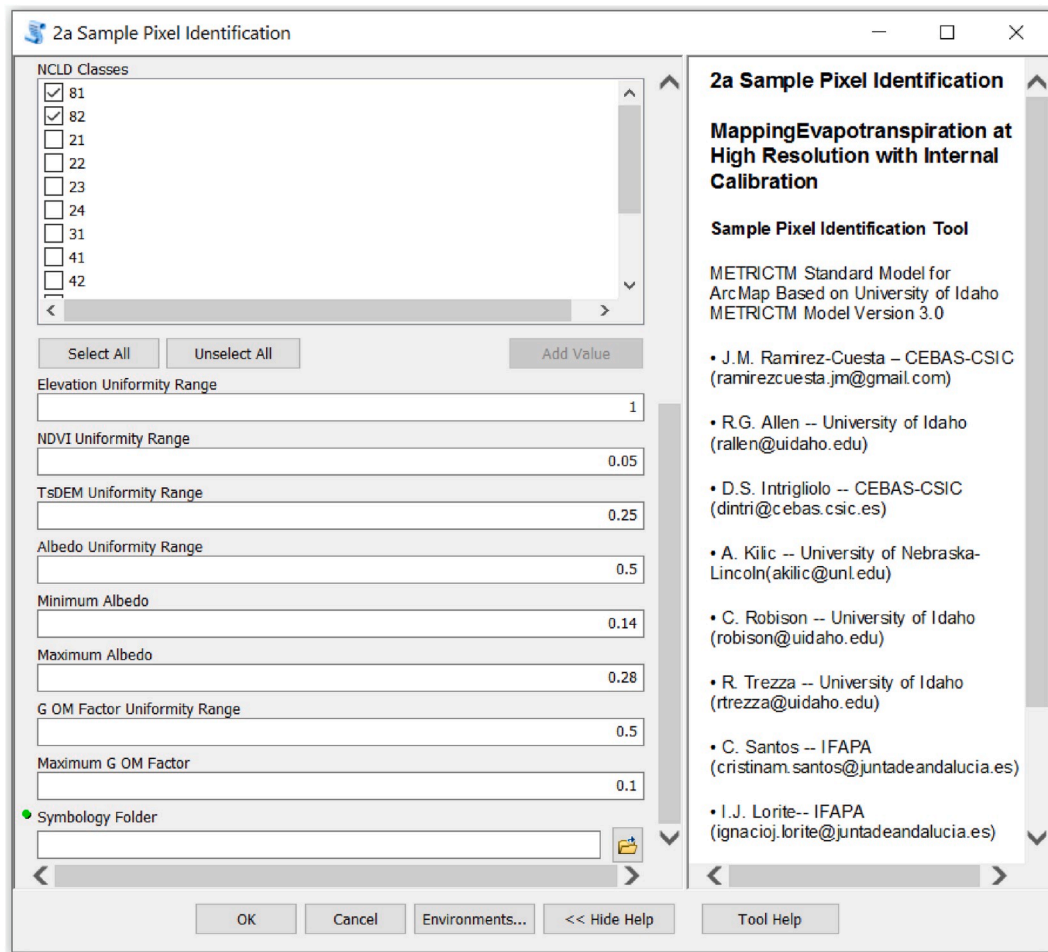


Fig. 2b. Section two of toolbox interface of sub-model 2, “2a. Sample Pixel Identification”, implemented in ArcGIS, showing the different input parameters. For definitions of the abbreviations used in the figure, readers are referred to the main text.

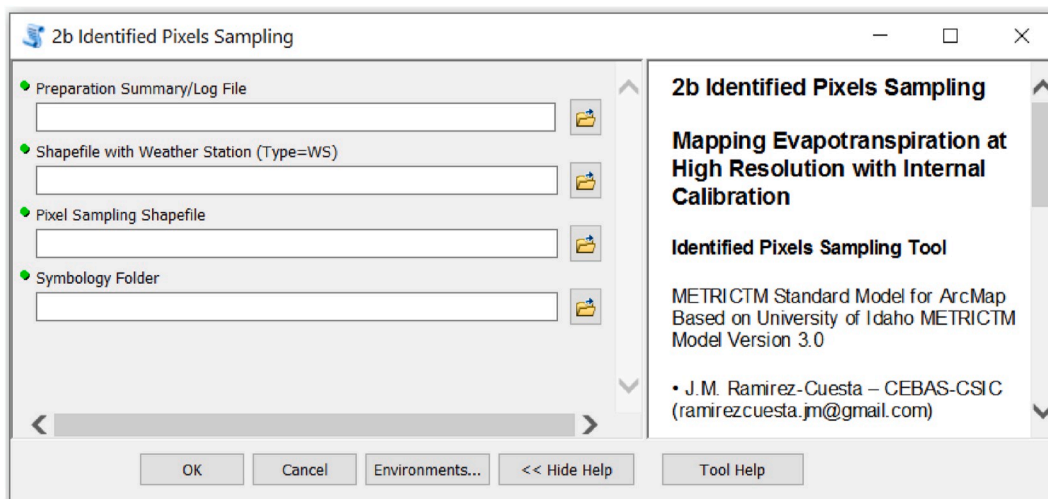


Fig. 3. Toolbox interface of sub-model 2, “2b. Identified Pixels Sampling”, implemented in ArcGIS, showing the different input parameters. For definitions of the abbreviations used in the figure, readers are referred to the main text.

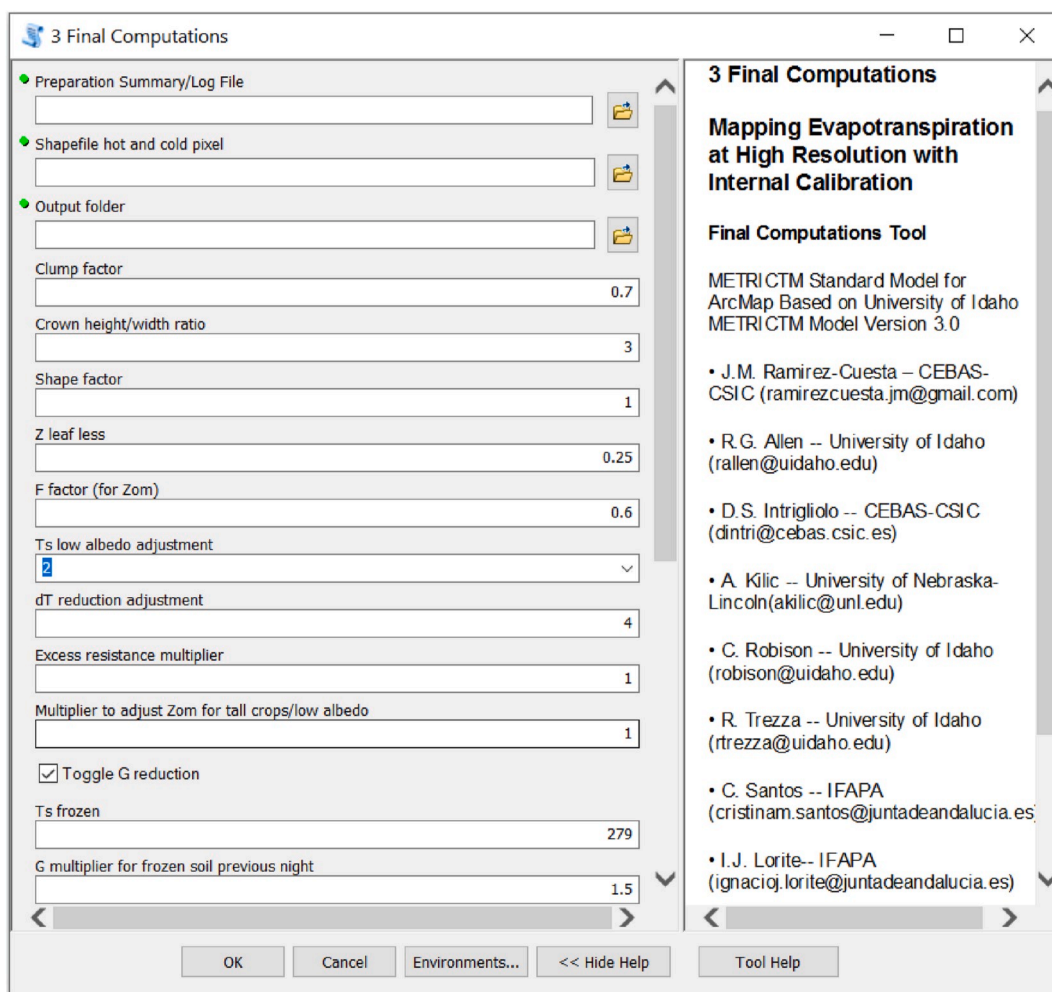


Fig. 4a. Section one of toolbox interface of sub-model 3, “3. Final Computations”, implemented in ArcGIS, showing the different input parameters. For definitions of the abbreviations used in the figure, readers are referred to the main text.

district are loamy soils. Primary crops in the area are wheat, cotton, olive, maize, sugar beet, beans, garlic, sunflower, and other vegetables. Irrigation water is provided using a modern pressurized irrigation network where users are able to control the frequency, rate and duration of water delivery. The irrigation system generally depends on the crop type, varying from manually operated sprinkler for wheat or sunflower to drip systems for maize, horticultural crops and olives.

In total, 25 maize fields, with an average area of 12 ha, were selected (Fig. 6) for comparisons against the FAO-56 $K_c ET_0$ method, occupying a total area of 290 ha approximately. Regarding the irrigation system, 80% of the fields were irrigated using drip systems whereas the other 20% were irrigated using sprinklers. The planting date ranged from late February to early April.

2.4.2. Remotely sensed data

The METRIC model requires a satellite image that includes thermal (T_s) information so Landsat satellites (Landsat 7 ETM+ and Landsat 8 OLI/TIRS) were utilized in this study. Landsat 7 bands 1–5 and 7; and Landsat 8 bands 2–7 refer to the visible and near-short wave infrared regions with 30 m spatial resolution, while Landsat 7 band 6 and Landsat 8 band 10 provide data for longwave (thermal) radiation. The spatial resolution of these thermal bands is 60 m for Landsat 7 and 100 m for Landsat 8 (Landsat Project Science Office (LPSO) 2006; 2015). The temporal resolution between Landsat overpasses is 16 days for each satellite, so a theoretical temporal resolution of 8 days was obtained in this study under clear sky conditions since the data provided by both

Landsat 7 and 8 satellites were combined. However, the absence of clouds in the area of interest in the satellite scene is a requirement for applying the METRIC model. Additionally, since 2003 Landsat 7 Scan Line Corrector is not working, resulting in data gaps in the image that sometimes included the experimental plots. Therefore, a significant number of available images containing clouds or affected by Scan Line Corrector failure over the study area had to be discarded, especially from April to June, reducing the final temporal resolution for the study. For the final analyses, ten clear sky images were used for the 2015 irrigation season (March–September 2015). Table 1 shows the Landsat scenes considered in this study (path 201 row 34).

2.4.3. Meteorological data

Semi-hourly air temperature, relative humidity, wind speed and direction, R_{so} and precipitation data was required for the 2015 irrigation season to run METRIC-GIS. These data were obtained from the Santaella weather station (37° 31.33' N, 4° 53.12' W) and were supplied by the Agroclimatic Information Network of Andalusia (Red de Información Agroclimática de Andalucía, RIA; Gavilán et al., 2006).

For this study, a Quality Analysis/Quality Control (QA/QC) was conducted on the semi-hourly values collected from the Santaella weather station. This analysis was performed using the QA/QC module v.2.0 of the RefET software v.4.1 (Allen, 2015; Li and Allen, 2015). The QA/QC process involved the visual analysis of reported R_{so} versus a theoretical clear sky estimate, visual comparison of air temperature with computed dewpoint temperature, and visual scanning of semi-hourly

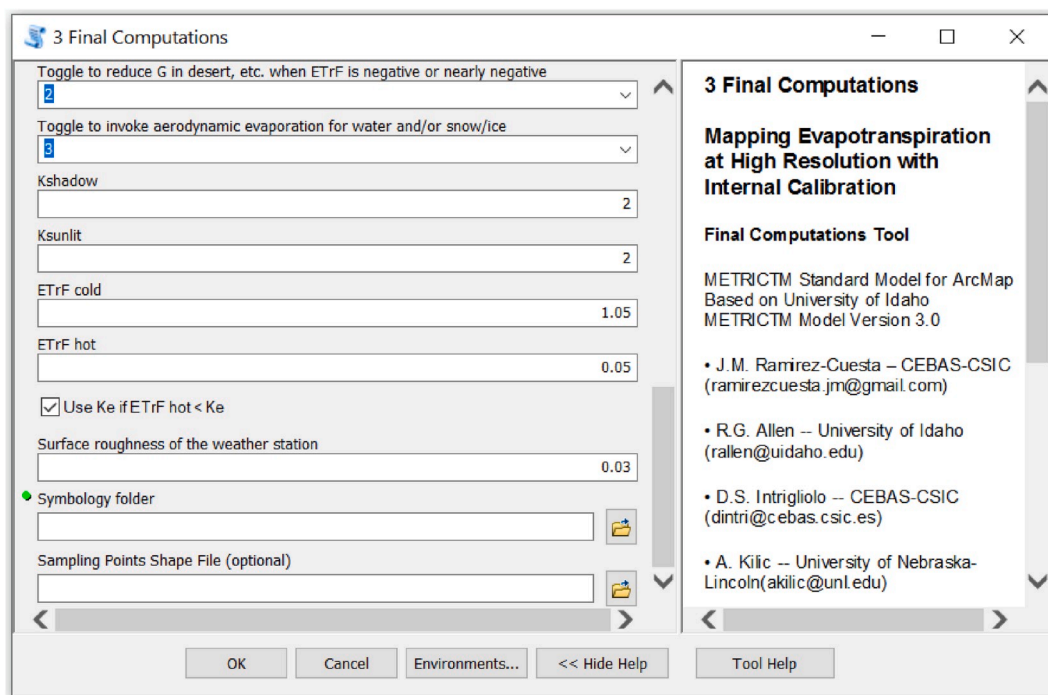


Fig. 4b. Section two of toolbox interface of sub-model 3, “3. Final Computations”, implemented in ArcGIS, showing the different input parameters. For definitions of the abbreviations used in the figure, readers are referred to the main text.

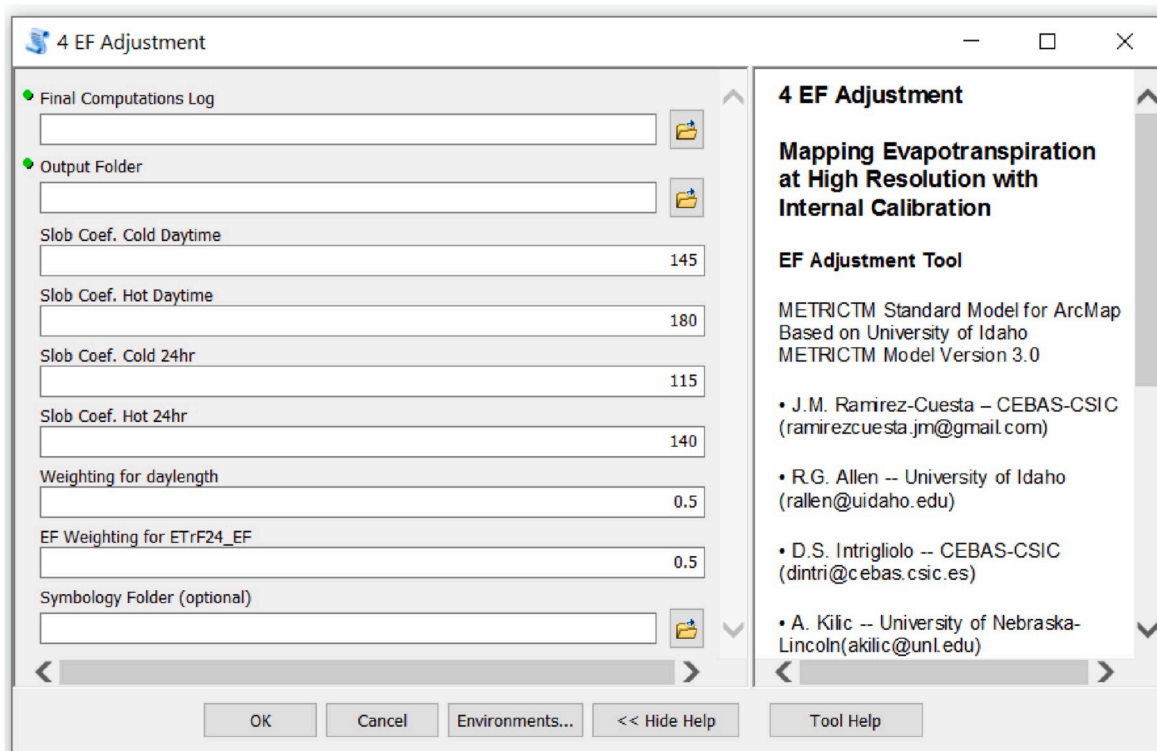


Fig. 5. Toolbox interface of sub-model 4, “4. EF Adjustment”, implemented in ArcGIS, showing the different input parameters. For definitions of the abbreviations used in the figure, readers are referred to the main text.

RH and wind speed data. Additionally, the RefET software (Allen, 2015) was used to calculate reference evapotranspiration using the FAO-56 Penman-Monteith equation applied to the alfalfa reference crop. The alfalfa reference is needed to establish maximum ET values in the image and to compute an hourly and daily soil water balance in METRIC that is

used to assign an ET value to a bare soil condition in the vicinity of the weather station. The alfalfa reference ET is generally 20–40% higher than the clipped grass reference ET (ASCE-EWRI, 2005).

Additionally, a theoretical crop coefficient curve for maize with K_c values tabulated from the FAO-56 document (Allen et al., 1998) for the

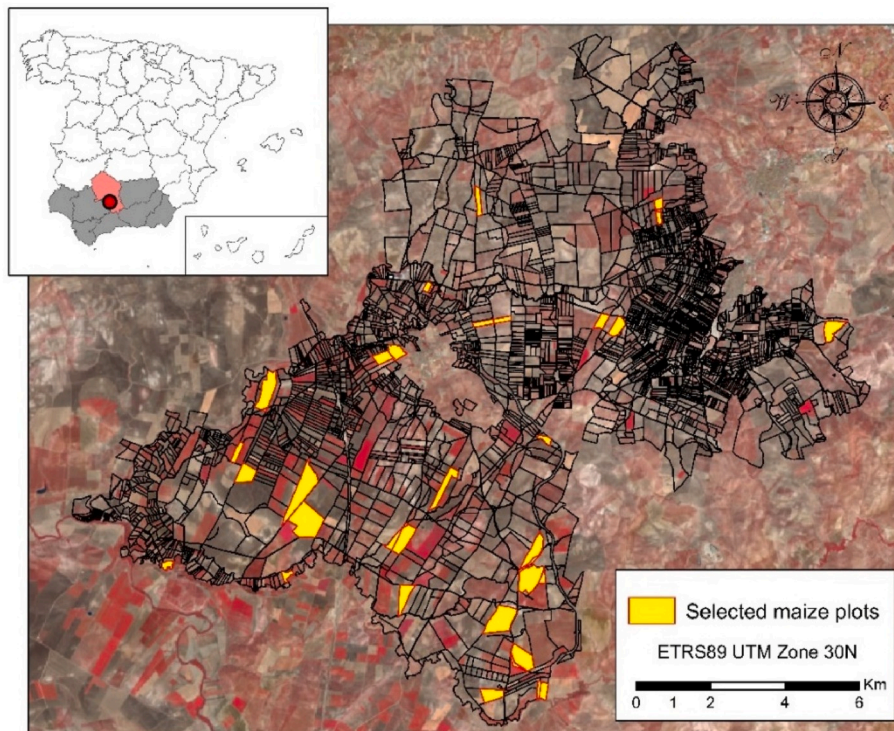


Fig. 6. Location of the Genil-Cabra Irrigation Scheme and the 25 maize fields (in yellow) used for METRIC-GIS performance evaluation and demonstration. The red colors in the Landsat false color image indicate dense green vegetation. (For interpretation of the references to color in this figure legend, the reader is referred to the Web version of this article.)

Table 1
Date and satellite of the Landsat scenes used in the study.

Date	DOY	Satellite
March 9th, 2015	68	Landsat 7
April 2nd, 2015	92	Landsat 8
June 29th, 2015	180	Landsat 7
July 7th, 2015	188	Landsat 8
July 15th, 2015	196	Landsat 7
July 23rd, 2015	204	Landsat 8
July 31st, 2015	212	Landsat 7
August 16th, 2015	228	Landsat 7
September 1st, 2015	244	Landsat 7
September 25th, 2015	268	Landsat 8

different maize crop stages was built and compared with the K_c curve obtained by sampling fields for ET produced by the METRIC-GIS application. A grass-reference-based K_c was computed from METRIC-GIS by dividing sampled ET by the grass reference ET. Due to the planting date variability among the 25 considered maize field, crop stages length used to build the theoretical K_c curve were determined by maintaining the proportion of each crop stage in relation to the total crop development stage length. The K_c values for initial ($K_{c, ini}$), mid ($K_{c, mid}$) and late-season ($K_{c, late}$) crop stages were 0.30, 1.20 and 0.50, respectively (Allen et al., 1998). Due to average climatic conditions in the study area for the considered period did not differ greatly from those indicated by Allen et al. (1998), no specific climatic adjustment was applied.

2.5. Statistical analysis

METRIC-GIS versus METRIC_{erdas} comparisons were assessed using mean bias error (ME; eq. (7)), root mean squared error (RMSE, eq. (8)), and coefficient of determination (R^2). Additionally, besides the above-mentioned statistical indicators, for the comparison between K_c curves derived from METRIC-GIS and from FAO56, the intercept and slope

terms of the obtained relationships were considered (a and b terms in a typical linear function, $y = a + bx$, respectively).

$$ME = \sum_{i=1}^n \frac{S_i - M_i}{n} \tag{7}$$

$$RMSE = \sqrt{\frac{\sum_{i=1}^n (S_i - M_i)^2}{n}} \tag{8}$$

3. Results

3.1. Practical validation

Fig. 7 shows the comparison between the energy balance components derived from METRIC_{erdas} and from METRIC-GIS. The performance of both versions was identical, with relationships for all major energy balance components coinciding with the 1:1 line (intercept and slope terms equal to 0.00 and 1.00, respectively), R^2 values equal to 1.00 and RMSE equal to 0.00 $W m^{-2}$ (or $mm day^{-1}$ for ET_c). Additionally, the different components derived from METRIC-GIS were unbiased, since ME was equal to 0 $W m^{-2}$ (or $mm day^{-1}$ for ET_c). Computationally, the time spent in the simulation using METRIC-GIS was 50% lower than when using METRIC_{erdas}.

3.2. Crop coefficients curves and variability analysis

Using METRIC-GIS, the energy balance components and K_c for each date were produced and sampled for the 25 maize fields evaluated. Averaging all plots during the irrigation season, R_n ranged from 404 to 631 $W m^{-2}$ over the irrigation season; G from 43 to 100 $W m^{-2}$, and H from 55 to 291 $W m^{-2}$. These values resulted in ET_c ranging from 0.88 (at the beginning of the season) to 9.55 $mm day^{-1}$ (at the end of July; DOY 204), and K_c ranging from 0.34 to 1.20, respectively. The spatial distribution of K_c for the days when clear-sky satellite images were

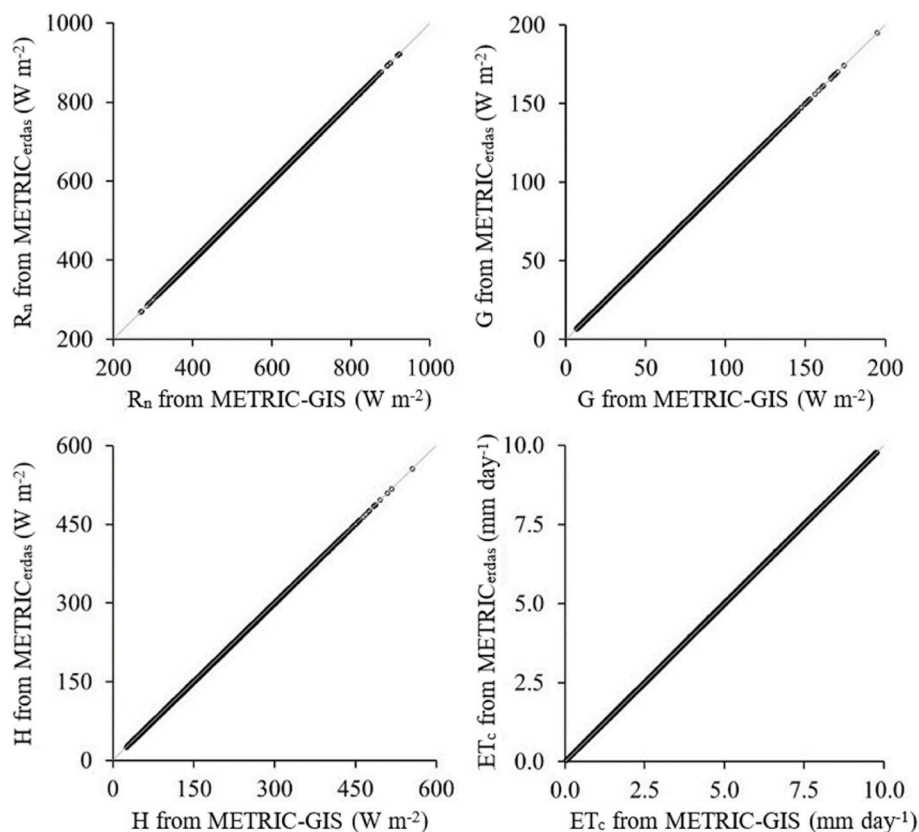


Fig. 7. Relationship between R_n , G , H and ET_c obtained from METRIC_{erdas} and METRIC-GIS for the Landsat 8 scene of the DOY 188 of 2015 (Path 201 Row 34). Grey lines represent the 1:1 relationships.

available is shown in Fig. 8.

Fig. 9 shows the temporal evolution of mean, minimum and maximum K_c values for the 25 maize fields during the irrigation season and the variability among fields. It is observed that the variation among fields was higher during the crop development stage and the late season stage due to differences in irrigation scheduling, crop development rates and spatial distribution of rainfall, whereas this variability was reduced during the mid-season stage when nearly all fields were at full ground cover. Variation among fields is represented by the different thicknesses of the grey areas (Fig. 9).

A RMSE value of 0.18 was obtained when comparing the mean K_c curve with the theoretical one proposed by Allen et al. (1998) over the ten image dates. Additionally, most of the time (56%), the theoretical K_c curve was included within the range of the observed K_c values (Fig. 9), experiencing a small underestimation during the initial and crop development stages (from DOY 83 to DOY 116; ME equal to -0.26) and a slight overestimation mainly during the mid-season stage (from DOY 155 to 185 and from DOY 210 to 240; ME equal to 0.21).

Additionally, an example of the intra-field variability is shown in Fig. 9, where the K_c values within the maize plot ranged from 0.15, coinciding with an area within the plot that was not cultivated; to values close to 1.08 in areas where the maize biomass was highest.

4. Discussion

METRIC-GIS has been able to reproduce traditional METRIC_{erdas} energy balance and ET estimates with lower computing time and using a simplified data entry and handling procedure for reducing potential user errors in the application of METRIC model.

METRIC-GIS has been able to assess the temporal evolution of K_c in accordance with the phenological development of maize. Low K_c values were obtained during the initial stage (≈ 0.6), increasing progressively

during the development phase reaching its maximum value during the mid-stage (≈ 1.0) and experiencing a decrease during the late phase. The maize K_c values derived from METRIC-GIS agreed with those proposed by Allen et al. (1998). Higher estimation observed during the crop development stages than with standard FAO56 approach may have been due to the occurrence of more rainfall during that period or more surface wetting from drip irrigation than is assumed in the standard FAO-56 single K_c value for the initial period. The period of maximum K_c from METRIC-GIS was much shorter than that estimated from FAO-56, where the peak period lasted only about 15 days (between two image dates) with METRIC-GIS as compared to about 70 days from FAO-56.

In addition, whereas METRIC-GIS determines the actual ET and therefore can be employed to identify non-optimal field conditions, the FAO-56 methodology assumes a pristine crop condition when developing crop coefficients and is not based on individual field observations. Previous studies in the area integrating field measurements, remote sensing and modelling have confirmed that maize is often not cultivated under optimal and full irrigation conditions in all the fields (Santos et al., 2008; García-Vila et al., 2008; Lorite et al., 2012). Thus, for fields cultivated with maize in the Genil-Cabra Irrigation Scheme, the average ratio between irrigation supply and optimal irrigation supply ranged between 0.8 and 1.0, but around 35% of the maize fields were irrigated under deficit irrigation strategies. The causes associated with farmer behavior are described in Lorite et al. (2012) and are mainly related to poor irrigation management carried out by the farmers. Thus, although a significant number of fields were managed under optimal conditions, a number of fields were managed under deficit irrigation strategies. This behavior is confirmed in our study. The elevated number of fields practicing deficit irrigation generated an averaged crop coefficient during mid-season that was below the values indicated in FAO56.

Another difference between METRIC-GIS and FAO56 methodologies lies in the way these approaches are extended to other regions with

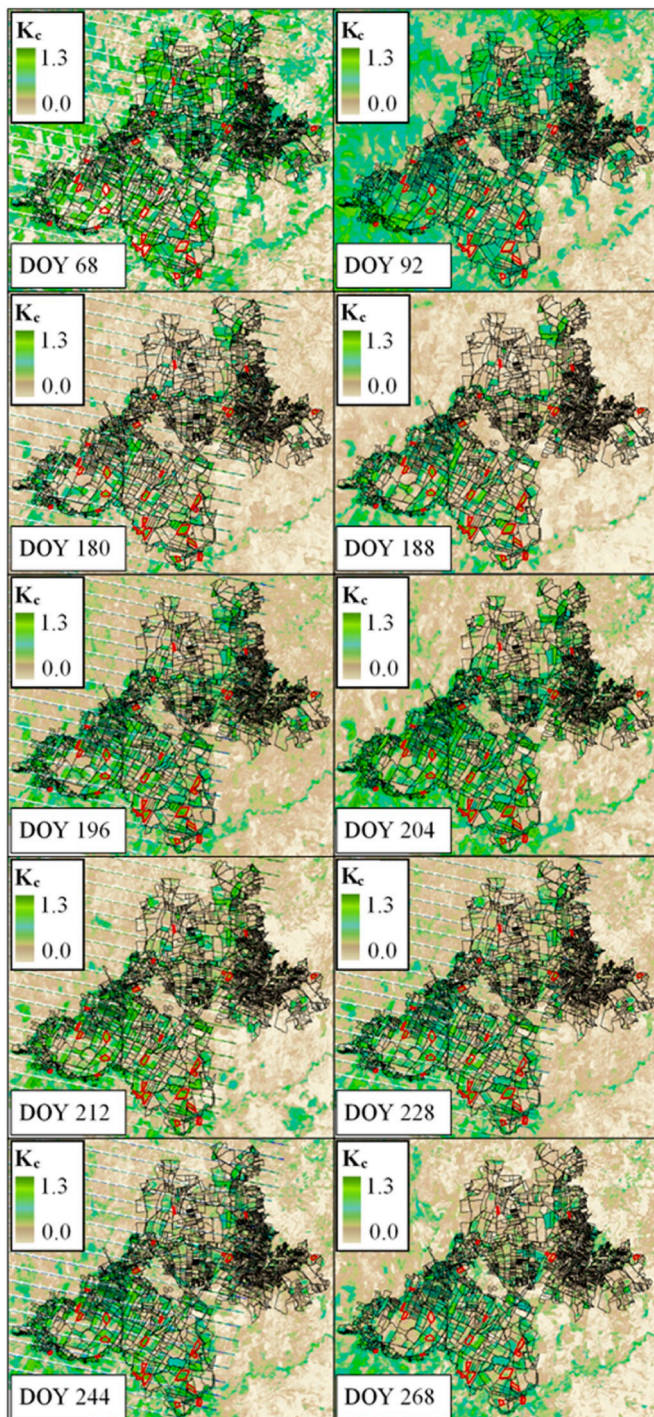


Fig. 8. Crop coefficient (K_c) image for a grass reference ET basis obtained from METRIC-GIS for each day considered in the study. Red outlines refer to the maize fields selected for comparison to the traditional FAO56 K_c method. (For interpretation of the references to color in this figure legend, the reader is referred to the Web version of this article.)

similar or different climates. Thus, whereas METRIC-GIS intrinsically considers the spatial/climate variability since it calibrates itself accordingly to the hot and cold pixel conditions (that change from place to place), the FAO56 approach needs to adjust K_c according to the specific meteorological conditions and local crop management and phenology (as indicated Allen et al. (1998)). Moreover, using METRIC-GIS allows the consideration of the spatial variability component, which is generally neglected when applying only numerical

methods (Allen et al., 1998) without field observations. This issue has been previously highlighted by other authors who have incorporated a spatial component into the FAO-56 approach by the utilization of remote sensing and GIS technologies (Gonzalez-Dugo et al., 2009; Campos et al., 2010; Santos et al., 2010; Ramírez-Cuesta et al., 2019a). The variability observed in K_c determined from METRIC-GIS among the analyzed maize fields was mainly due to differences in the irrigation amount, crop management practices, planting and harvesting dates, and soil characteristics; which influenced the crop development status of the different maize fields for each satellite date. The identification of this variability is uniquely possible considering tools as remote sensing, that evaluate huge areas at the same time with the same sensors.

The results obtained from the METRIC-GIS toolbox were the same as those from METRIC_{erdas}. The use of METRIC-GIS removes the need for using an external spreadsheet and lets the user introduce more easily the required inputs, using a user-friendly interface. Additionally, in models performing internalized calibrations, as METRIC-GIS, the proper selection of the anchor pixels results critical. Thus, the identification of potential calibration and pixels review as facilitated with the new tool provides a useful alternative to ensure that selected pixels meet the established requirements (Kjaersgaard et al., 2009; Allen et al., 2013a). In addition, ArcGIS licenses and software are more commonly in use than ERDAS. METRIC_{erdas} follows the perspective of many models developed for research purposes, which do not pay as much special attention to the model usability, being more focused on the model background and development (Jones et al., 2016). However, visualization and user-friendliness of output products are critical for end-users, including new users (Antle et al., 2017; Huang et al., 2018). METRIC-GIS pays special attention to this need, with outputs automatically added with an appropriate symbology and using a common raster format (Tagged Image File Format; TIF) to the viewer window of ArcGIS. This results in easier interpretation and analysis of the outputs for a non-specialized user. Additionally, this format allow managing METRIC-GIS outputs in other image processing software (eCognition, ENVI, ERDAS Imagine, IDRISI or PCI Geomatica), which favors the interoperability of the results obtained. Future improvements will include the automation of the satellite image downloading, and the adaptation of the model to be used with high-resolution images obtained from aircraft or drone. This will reduce user-intervention requirements, facilitating the use of METRIC-GIS by less experienced operators. Regarding the METRIC algorithm itself, this model was originally developed for being applied over relatively homogeneous crops having full-vegetated ground cover. However, more research is needed in relation to the characterization of heterogeneous systems where the energy balance is more complex (Santos et al., 2012; Jimenez-Bello et al., 2015), especially when coarse pixel sizes are used, not being possible to quantify within tree canopy variability. In this regard, the enhancement of the spatial resolution resulting from using aircraft or drones will allow identifying multiple pure pixel within a single tree canopy (Gonzalez-Dugo et al., 2012; Conesa et al., 2019).

Under mountain terrain conditions, components of sensible heat transfer such as roughness length, showed higher variability, and then, higher uncertainties in the outputs model were identified (Allen and Trezza, 2011). Moreover, most of the agricultural areas located at mountain areas are impacted by additional uncertainties such as the study of woody crops considering energy balance approaches based on satellite images (Santos et al., 2012). Due to these limitations, the METRIC version for flat areas, a more validated and simpler version, was considered in this study for facilitating the widespread use of METRIC in agricultural areas.

The analysis of large irrigation districts considering simulation models often requires long processing times, especially for complex models. This issue has been pointed out as an important limitation in the use of many other models (Jones et al., 2016; Longo et al., 2016; Ding et al., 2018). The incorporation of METRIC into a geographic information system (GIS) as METRIC-GIS reduced computational time by up to

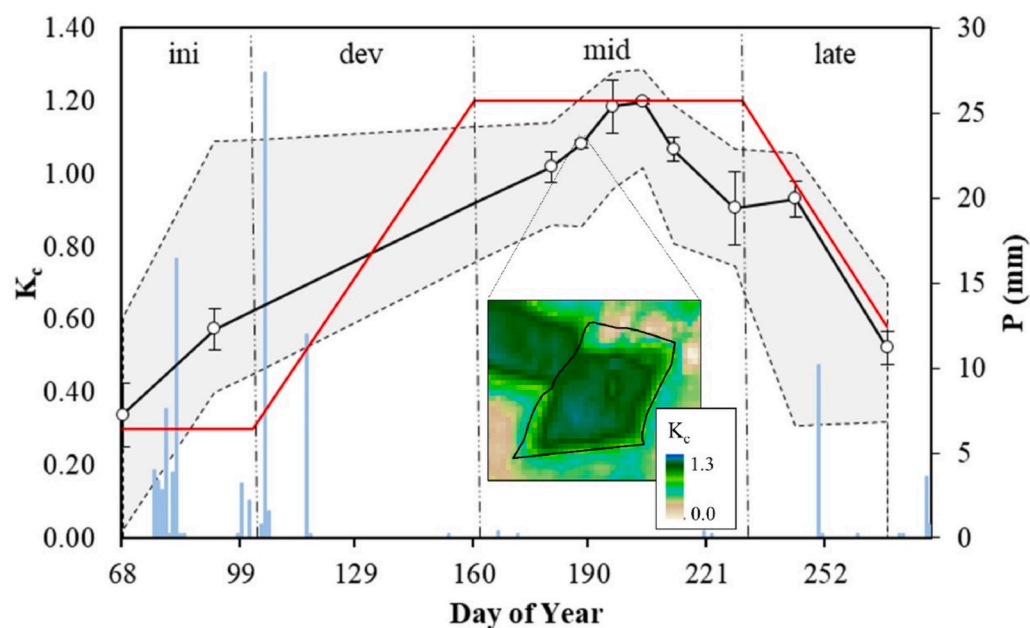


Fig. 9. Temporal evolution of the mean (solid black line), range (grey area), and standard deviation (whiskers) for K_c over the 25 maize fields evaluated obtained from METRIC-GIS, and precipitation (vertical blue bars). The red line represents the theoretical FAO-56-based curve for maize adjusted for the observed growth stages length. Ini, dev, mid and late refer to initial, development, mid and late-season crop stages, respectively. White dots represent DOY when a clear-sky satellite image was available. The raster in the Figure corresponds with an example of K_c map in a single maize field for the DOY 188. (For interpretation of the references to color in this figure legend, the reader is referred to the Web version of this article.)

50% when compared with METRIC_{erdas}, providing an additional advantage in the use of the proposed tool. Currently, METRIC-GIS is implemented in ArcGIS because this software is one of the most used GIS worldwide for environmental modelling processes (Zeng et al., 2007; Maguire, 2008; Roberts et al., 2010; Panda et al., 2019; Feng et al., 2020). Nonetheless, since ArcGIS uses python as a programming language, METRIC-GIS can be migrated to other platforms using the same language (e.g. open-software systems such as Quantum Geographical Information System; QGIS), expanding the operational possibilities of the tool.

The developed tool aims to be an alternative to the already existing platforms that use METRIC, as the case of the Earth Engine Evapotranspiration Flux, EEFlux, on the Google Earth Engine (Allen et al., 2015; Foolad et al., 2018). One of the major differences between EEFlux or other solutions able to process hundreds of satellite images at once (Cunha et al., 2020) and the METRIC-GIS tool developed in this manuscript lies in the way the extreme pixels are determined. In the METRIC-GIS tool, “2a. Sample Pixel Identification” and “2b. Identified Pixels Sampling” sub-models are used for the identification of potential calibration and review pixels (Kjaersgaard et al., 2009; Allen et al., 2013a). The manual anchor pixel selection approach is also allowed in order to avoid possible uncertainties derived from automatic selection and also to provide the users more flexibility when running the model (for example, modifying the K_c values assigned to the extreme pixels). Additionally, METRIC-GIS allows expanding or refining the user-selected options in case reanalysis of the current images is required. In addition, neither internet connection (if the satellite images has been previously downloaded) nor license agreements (other than the software ArcGIS license) are required.

5. Conclusion

In this study, a novel ArcGIS toolbox implementing the METRIC energy balance model, named METRIC-GIS, was developed and tested in a semi-arid environment (Cordoba, Spain). The energy balance components obtained from METRIC-GIS were validated with values derived from the original METRIC_{erdas} version and resultant K_c values were compared with those proposed by the FAO-56 approach. The main key-points to be drawn from this study are:

- Energy balance components simulated with METRIC-GIS were identical to values obtained when using METRIC_{erdas}, eliminating the need for the ERDAS modelmaker system and the use of an external spreadsheet. The METRIC-GIS implementation also facilitates the input introduction reducing potential user errors.
- Computational time was reduced by up to 50% using METRIC-GIS when compared with METRIC_{erdas}.
- The identification of potential calibration and pixels review as facilitated with the new tool provides a useful alternative to ensure that selected pixels meet the established requirements.
- Maize K_c values derived from METRIC-GIS agreed statistically with those tabulated in the FAO-56 document, with the advantage of providing information regarding the spatial component related to irrigation/agronomical management at field scale.

Declaration of competing interest

The authors declare that they have no known competing financial interests or personal relationships that could have appeared to influence the work reported in this paper.

Acknowledgments

This research was funded by the projects RTA2011-00015-00-00 funded by the National Institute for Agricultural and Food Research and Technology (INIA) and FEDER 2014–2020 “Programa Operativo de Crecimiento Inteligente” and by the European Commission with project “SHUI” (grant number: 773903). Additional funding support was provided by the Nebraska Agricultural Experiment Station and Idaho Agricultural Experiment Station.

References

- Allen, R.G., Pereira, L.S., Raes, D., Smith, M., 1998. Crop Evapotranspiration: Guidelines for Computing Crop Water Requirements. FAO Irrigation and Drainage Paper n° 56, FAO Irrigation and Drainage Paper. Roma.
- Allen, R.G., Tasumi, M., Morse, A., Trezza, R., 2005a. A Landsat-based energy balance and evapotranspiration model in Western US water rights regulation and planning. *Irrigat. Drain. Syst.* 19, 251–268.
- Allen, R.G., Tasumi, M., Trezza, R., 2005b. METRIC: Mapping Evapotranspiration at High Resolution – Applications Manual for Landsat Satellite Imagery. University of Idaho, p. 130.

- Allen, R.G., Tasumi, M., Trezza, R., 2007a. Satellite-based energy balance for mapping evapotranspiration with internalized calibration (METRIC)- model. *J. Irrigat. Drain. Eng.* 380–394.
- Allen, R.G., Kjaersgaard, J., 2010. Development of a Three-Source Temperature Model for Tall Orchards. In-Office White Paper. University of Idaho, Kimberly, Idaho, p. 14.
- Allen, R.G., Trezza, R., 2011. Adjustment to Aerodynamic Roughness, Aerodynamic Resistance and Wind Speed in Mountains. Working Memorandum. University of Idaho, Kimberly Research and Extension Center, p. 17p. Feb. 22-25, 2011.
- Allen, R., Irmak, A., Trezza, R., Hendrickx, J.M., Bastiaanssen, W., Kjaersgaard, J., 2011. Satellite-based ET estimation in agriculture using SEBAL and METRIC. *Hydrol. Process.* 25, 4011–4027.
- Allen, R.G., Tasumi, M., Morse, A., Trezza, R., Wright, J.L., Bastiaanssen, W., Kramber, W., Lorite, I., Robison, C.W., 2007b. Satellite-based energy balance for mapping evapotranspiration with internalized calibration (METRIC) - applications. *J. Irrigat. Drain. Eng.* 395–406.
- Allen, R.G., Burnett, B., Kramber, W., Huntington, J., Kjaersgaard, J., Kilic, A., Kelly, C., Trezza, R., 2013a. Automated calibration of the METRIC-landsat evapotranspiration process. *J. Am. Water Resour. Assoc.* 49, 563–576.
- Allen, R.G., Trezza, R., Kilic, A., Tasumi, M., Li, H., 2013b. Sensitivity of landsat-scale energy balance to aerodynamic variability in mountains and complex terrain. *JAWRA Journal of the American Water Resources Association* 49, 592–604.
- Allen, R.G., 2015. Ref-ET: Reference Evapotranspiration Calculation Software for FAO and ASCE Standardized Equations. University of Idaho: Kimberly, ID, USA.
- Allen, R.G., Morton, C., Kamble, B., Kilic, A., Huntington, J., Thau, D., Gorelick, N., et al., 2015. EEFlux: a landsat-based evapotranspiration mapping tool on the Google Earth engine. In: 2015 ASABE/IA Irrigation Symposium: Emerging Technologies for Sustainable Irrigation-A Tribute to the Career of Terry Howell, Sr. Conference Proceedings. American Society of Agricultural and Biological Engineers, pp. 1–11.
- Anderson, M.C., Norman, J.M., Diak, G.R., Kustas, W.P., Mecikalski, J.R., 1997. A two-source time-integrated model for estimating surface fluxes using thermal infrared remote sensing. *Remote Sens. Environ.* 60, 195–216.
- Antle, J.M., Jones, J.W., Rosenzweig, C.E., 2017. Next generation agricultural system data, models and knowledge products: Introduction. *Agric. Syst.* 155, 186–190.
- ASCE-EWRI, 2005. In: Allen, R.G., Walter, I.A., Elliott, R., Howell, T., Itenfisu, D., Jensen, M. (Eds.), *The ASCE Standardized Reference Evapotranspiration Equation. Final Report (ASCE-EWRI) Pr. Environmental and Water Resources Institute, American Society of Civil Engineers*, p. 74.
- Atasever, U.H., Kesikoglu, M.H., Özkan, C., 2013. EvaMapper: a novel MATLAB toolbox for evapotranspiration mapping. *Int. Arch. Photogram. Rem. Sens. Spatial Inf. Sci.* 7, W2.
- Bastiaanssen, W.G.M., 1995. Regionalization of Surface Flux Densities and Moisture Indicators in Composite Terrain: a Remote Sensing Approach under Clear Skies in Mediterranean Climates. Wageningen University.
- Bastiaanssen, W.G.M., Menenti, M., Feddes, R.A., Holtslag, A.A.M., 1998. A remote sensing surface energy balance algorithm for land (SEBAL). 1. Formulation. *J. Hydrol.* 212–213, 198–212.
- Bastiaanssen, W.G.M., Noordman, E.J.M., Pelgrum, H., Davids, G., Thoreson, B.P., Allen, R.G., 2005. SEBAL model with remotely sensed data to improve water-resources management under actual field conditions. *J. Irrigat. Drain. Eng.* 131, 85–93.
- Betts, A.K., Chen, F., Mitchell, K.E., Janjic, Z.I., 1997. Assessment of the land surface and boundary layer models in two operational versions of the NCEP Eta model using FIFE data. *Mon. Weather Rev.* 125, 2896–2916.
- Bhattarai, N., Liu, T., 2019. LandMOD ET mapper: a new matlab-based graphical user interface (GUI) for automated implementation of SEBAL and METRIC models in thermal imagery. *Environ. Model. Software* 118, 76–82.
- Brutsaert, W., 1982. Evaporation into the Atmosphere. D. Reidel Pub. Co., Boston, p. 309.
- Campos, I., Neale, C.M., Calera, A., Balbontin, C., González-Piqueras, J., 2010. Assessing satellite-based basal crop coefficients for irrigated grapes (*Vitis vinifera* L.). *Agric. Water Manag.* 98, 45–54.
- Conesa, M.R., Conejero, W., Vera, J., Ramírez-Cuesta, J.M., Ruiz-Sánchez, M.C., 2019. Terrestrial and remote indexes to assess moderate deficit irrigation in early-maturing nectarine trees. *Agronomy* 9 (10), 630.
- Courault, D., Seguin, B., Olioso, A., 2005. Review on estimation of evapotranspiration from remote sensing data: from empirical to numerical modeling approaches. *Irrigat. Drain. Syst.* 19, 223–249.
- Cunha, J., Pereira, T.E., Pereira, E., Rufino, I., Galvão, C., Valente, F., Brasileiro, F., 2020. A high-throughput shared service to estimate evapotranspiration using Landsat imagery. *Comput. Geosci.* 134, 104341.
- Ding, Y., Wang, L., Li, Y., Li, D., 2018. Model predictive control and its application in agriculture: a review. *Comput. Electron. Agric.* 151, 104–117.
- Drexler, J.Z., Snyder, R.L., Spano, D., Paw, U.K.T., 2004. A review of models and micrometeorological methods used to estimate wetland evapotranspiration. *Hydrol. Process.* 18, 2071–2101.
- ERDAS Imagine, 2014. ERDAS: Earth Resources Data Analysis System 2014. ERDAS, Inc. Norcross, GA, USA.
- Feng, Q., Flanagan, D.C., Engel, B.A., Yang, L., Chen, L., 2020. GeoAPEXOL, a web GIS interface for the Agricultural Policy Environmental eXtender (APEX) model enabling both field and small watershed simulation. *Environ. Model. Software* 123, 104569.
- Fereres, E., Soriano, M.A., 2007. Deficit irrigation for reducing agricultural water use. *J. Exp. Bot.* 58, 147–159.
- Food and Agriculture Organization (FAO), 2012. Coping with Water Scarcity: an Action Framework for Agriculture and Food Security. FAO Water Report 38. Rome.
- Foolad, F., Blankenau, P., Kilic, A., Allen, R.G., Huntington, J.L., Erickson, T.A., Ozturk, D., Morton, C.G., Ortega, S., Ratcliffe, I., Franz, T.E., Thau, D., Moore, R., Gorelick, N., Kamble, B., Revell, P., Trezza, R., Zhao, W., Robison, C.W., 2018. Comparison of the Automatically Calibrated Google Evapotranspiration Application—EEFlux and the Manually Calibrated METRIC Application. Preprints, 2018070040.
- García-Vila, M., Lorite, I.J., Soriano, M.A., Fereres, E., 2008. Management trends and responses to water scarcity in an irrigation scheme of Southern Spain. *Agric. Water Manag.* 95, 458–468.
- Gavilán, P., Lorite, I.J., Tornero, S., Berengena, J., 2006. Regional calibration of Hargreaves equation for estimating reference ET in a semiarid environment. *Agric. Water Manag.* 81, 257–281.
- Gonzalez-Dugo, M.P., Neale, C.M.U., Mateos, L., Kustas, W.P., Prueger, J.H., Anderson, M.C., Li, F., 2009. A comparison of operational remote sensing-based models for estimating crop evapotranspiration. *Agric. For. Meteorol.* 149, 1843–1853.
- Gonzalez-Dugo, V., Zarco-Tejada, P., Berni, J.A., Suárez, L., Goldhamer, D., Fereres, E., 2012. Almond tree canopy temperature reveals intra-crown variability that is water stress-dependent. *Agric. For. Meteorol.* 154, 156–165.
- Goward, S., Cruickshanks, G.D., Hope, A., 1985. Observed relation between thermal emission and reflected spectral radiance of a complex vegetated landscape. *Remote Sens. Environ.* 18, 137–146.
- Healey, N.C., 2011. Analyzing Ecohydrology of Subirrigated Meadow, Dry Valley and Upland Dune Ecosystems Using Remote Sensing and In-Situ Estimations in the Semiarid Sand Hills Region of Nebraska. Ph.D. Dissertation. University of Nebraska - Lincoln, USA.
- Hessels, T., van Opstal, J., Trambauer, P., Bastiaanssen, W., Faouzi, M., Mohamed, Y., ErRaji, A., 2017. pySEBAL Version 3.3.7.
- Huang, Y., Chen, Z.X., Tao, Y., Huang, X.Z., Gu, X.F., 2018. Agricultural remote sensing big data: management and applications. *Journal of Integrative Agriculture* 17, 1915–1931.
- Irmak, A., Ratcliffe, I., Ranade, P., Hubbard, K.G., Singh, R.K., Kamble, B., Kjaersgaard, J., 2011. Estimation of land surface evapotranspiration with a satellite remote sensing procedure. *Great Plains Res.* 21, 73–88.
- Jiménez-Bello, M.Á., Castel, J.R., Testi, L., Intrigliolo, D.S., 2015. Assessment of a remote sensing energy balance methodology (SEBAL) using different interpolation methods to determine evapotranspiration in a citrus orchard. *IEEE Journal of Selected Topics in Applied Earth Observations and Remote Sensing* 8 (4), 1465–1477.
- Jones, J.W., Antle, J.M., Basso, B., Boote, K.J., Conant, R.T., Foster, I., Godfray, H.C.J., Herrero, M., Howitt, R.E., Janssen, S., Keating, B.A., Muñoz-Carpena, R., Porter, C. H., Rosenzweig, C., Wheeler, T.R., 2016. Brief history of agricultural systems modeling. *Agric. Syst.* 155, 240–254.
- Jovanovic, N., Israel, S., 2012. Critical review of methods for the estimation of actual evapotranspiration in hydrological models. In: Irmak, A. (Ed.), *Evapotranspiration-Remote Sensing and Modeling*. InTech, pp. 329–350.
- Kilic, A., Allen, R., Trezza, R., Ratcliffe, I., Kamble, B., Robison, C., Ozturk, D., 2016. Sensitivity of evapotranspiration retrievals from the METRIC processing algorithm to improved radiometric resolution of Landsat 8 thermal data and to calibration bias in Landsat 7 and 8 surface temperature. *Rem. Sens. Environ.* 185, 198–209.
- Kjaersgaard, J.H., Allen, R.G., Trezza, R., Garcia, M., Kramber, W., 2009. Automated selection of anchor pixels for Landsat-based evapotranspiration estimation. In: *ASCE World Environmental and Water Resources Congress Proceedings*. Kansas City, Missouri.
- Kustas, W.P., Norman, J.M., Anderson, M.C., French, A.N., 2003. Estimating subpixel surface temperatures and energy fluxes from the vegetation index-radiometric temperature relationship. *Remote Sens. Environ.* 85, 429–440.
- Lagos, L.O., Merino, G., Martin, D., Verma, S., Suyker, A., 2011. Evapotranspiration of partially vegetated surfaces. In: Irmak, A. (Ed.), *Evapotranspiration-Remote Sensing and Modeling*. InTech, pp. 273–304.
- Landsat Project Science Office (LPSO), 2006. *Landsat 7 Science Data Users' Handbook*. Landsat Project Science Office. NASA Goddard Space Flight Center, Greenbelt, Md.
- Landsat Project Science Office (LPSO), 2015. *Landsat 8 Science Data Users' Handbook*. Landsat Project Science Office. NASA Goddard Space Flight Center, Greenbelt, Md.
- Li, G., Allen, R.G., 2015. Ref-ET-QAQC: QAQC Weather Data from RefET with Excel Graphics. University of Idaho: Kimberly, ID, USA.
- Liu, J., 2009. A GIS-based tool for modelling large-scale crop-water relations. *Environ. Model. Software* 24 (3), 411–422.
- Longo, M., Arroqui, M., Rodriguez, J., Machado, C., Mateos, C., Zunino, A., 2016. Extending JASAG with data processing techniques for speeding up agricultural simulation applications: a case study with Simugan. *Information Processing in Agriculture* 3, 235–243.
- Lorite, I.J., García-Vila, M., Carmona, M.A., Santos, C., Soriano, M.A., 2012. Assessment of the irrigation advisory services' recommendations and farmers' irrigation management: a case study in southern Spain. *Water Resour. Manag.* 26, 2397–2419.
- Lorite, I.J., García-Vila, M., Santos, C., Ruiz-Ramos, M., Fereres, E., 2013. AquaData and AquaGIS: two computer utilities for temporal and spatial simulations of water-limited yield with AquaCrop. *Comput. Electron. Agric.* 96, 227–237.
- Maguire, D., 2008. ArcGIS: general purpose GIS software system. In: Shekhar, S., Xiong, H. (Eds.), *Encyclopedia of GIS*. Springer, Boston, MA.
- Mendicino, G., Versace, P., 2007. Integrated drought watch system: a case study in Southern Italy. *Water Resour. Manag.* 21, 1409–1428.
- Moran, M.S., Clarke, T.R., Inoue, Y., Vidal, A., 1994. Estimating crop water deficit using the relationship between surface-air temperature and spectral vegetation index. *Remote Sens. Environ.* 49, 246–363.
- Nemani, R.R., Running, S.W., 1989. Estimation of regional surface resistance to evapotranspiration from NDVI and thermal-IR AVHRR Data. *J. Appl. Meteorol.* 28, 276–284.

- Norman, J.M., Kustas, W.P., Humes, K.S., 1995. A two-source approach for estimating soil and vegetation energy fluxes from observations of directional radiometric surface temperature. *Agric. For. Meteorol.* 77, 263–293.
- Owusu, G., 2016. Surface energy balance and crop coefficient estimation with R. Available from: <https://rdrr.io/github/gowusu/sebkc/>. Accessed June 08, 2020.
- Panda, S.S., Amatya, D.M., Muwamba, A., Chescheir, G., 2019. Estimation of evapotranspiration and its parameters for pine, switchgrass, and intercropping with remotely-sensed images based geospatial modeling. *Environ. Model. Software* 121, 104487.
- Pereira, L.S., Gonçalves, J.M., Dong, B., Mao, Z., Fang, S.X., 2007. Assessing basin irrigation and scheduling strategies for saving irrigation water and controlling salinity in the upper Yellow River Basin, China. *Agric. Water Manag.* 93, 109–122.
- Perrier, A., 1982. Land surface processes: vegetation, 395–448. In: Eagleson, P. (Ed.), *Land Surface Processes in Atmospheric General Circulation Models*. Cambridge Univ. Press.
- Poblete-Echeverría, C., Ortega-Farías, S., 2012. Calibration and validation of a remote sensing algorithm to estimate energy balance components and daily actual evapotranspiration over a drip-irrigated Merlot vineyard. *Irrigat. Sci.* 30, 537–553.
- Raes, D., Steduto, P., Hsiao, T.C., Fereres, E., 2009. AquaCrop – the FAO crop model to simulate yield response to water: II. Main algorithms and software description. *Agron. J.* 101, 438–447.
- Ramírez-Cuesta, J.M., Mirás-Avalos, J.M., Rubio-Asensio, J.S., Intrigliolo, D.S., 2019a. A novel ArcGIS toolbox for estimating crop water demands by integrating the dual crop coefficient approach with multi-satellite imagery. *Water* 11, 38. <https://doi.org/10.3390/w11010038>.
- Ramírez-Cuesta, J.M., Allen, R.G., Zarco-Tejada, P.J., Kilic, A., Santos, C., Lorite, I.J., 2019b. Impact of the spatial resolution on the energy balance components on an open-canopy olive orchard. *Int J Appl Earth Obs Geoinformation* 74, 88–102.
- Rana, G., Katerji, N., 2000. Measurement and estimation of actual evapotranspiration in the field under Mediterranean climate: a review. *Eur. J. Agron.* 13, 125–153.
- Roberts, J.J., Best, B.D., Dunn, D.C., Trembl, E.A., Halpin, P.N., 2010. Marine geospatial ecology tools: an integrated framework for ecological geoprocessing with ArcGIS, Python, R, MATLAB, and C++. *Environ. Model. Software* 25 (10), 1197–1207.
- Roerink, G.J., Su, Z., Menenti, M., 2000. S-SEBI: a simple remote sensing algorithm to estimate the surface energy balance. *Phys. Chem. Earth B* 25, 147–157.
- Santos, C., Lorite, I.J., Tasumi, M., Allen, R.G., Fereres, E., 2008. Integrating satellite-based evapotranspiration with simulation models for irrigation management at the scheme level. *Irrigat. Sci.* 26, 277–288.
- Santos, C., Lorite, I.J., Tasumi, M., Allen, R.G., Fereres, E., 2010. Performance assessment of an irrigation scheme using indicators determined with remote sensing techniques. *Irrigat. Sci.* 28, 461–477.
- Santos, C., Lorite, I.J., Allen, R.G., Tasumi, M., 2012. Aerodynamic parameterization of the satellite-based energy balance (METRIC) model for ET estimation in rainfed olive orchards of Andalusia, Spain. *Water Resour. Manag.* 26, 3267–3283.
- Senay, G.B., Leake, S., Nagler, P.L., Artan, G., Dickinson, J., Cordova, J.T., Glenn, E.P., 2011. Estimating basin scale evapotranspiration (ET) by water balance and remote sensing methods. *Hydrol. Processes* 25, 4037–4049.
- Silva, C.D.O.F., de Castro Teixeira, A.H., Manzione, R.L., 2019. Agriwater: an R package for spatial modelling of energy balance and actual evapotranspiration using satellite images and agrometeorological data. *Environ. Model. Software* 120, 104497.
- Su, Z., 2002. The surface energy balance system (SEBS) for estimation of turbulent heat fluxes. *Hydrol. Earth Syst. Sci.* 6, 85–99.
- Tasumi, M., 2003. Progress in Operational Estimation of Regional Evapotranspiration Using Satellite Imagery. Ph.D. Dissertation. University of Idaho, Moscow, ID.
- Thorp, K.R., Marek, G.W., DeJonge, K.C., Evett, S.R., Lascano, R.J., 2019. Novel methodology to evaluate and compare evapotranspiration algorithms in an agroecosystem model. *Environ. Model. Software* 119, 214–227.
- Wigmosta, M.S., Vail, L., Lettenmaier, D.P., 1994. A distributed hydrology vegetation model for complex terrain. *Water Resour. Res.* 30, 1665–1679.
- Zeng, H., Talkkari, A., Peltola, H., Kellomäki, S., 2007. A GIS-based decision support system for risk assessment of wind damage in forest management. *Environ. Model. Software* 22 (9), 1240–1249.